

IDENTIFICATION AND VISUALIZATION OF VORTICES IN BY-PASS GRAFT FLOW

Alin F. TOTOREAN¹, Alin I. BOSIOC², Sandor I. BERNAD², Romeo SUSAN-RESIGA¹

¹ “Politehnica” University of Timisoara, Department of Hydraulic, RO-300222 Timisoara, Romania

² Centre of Advanced Research in Engineering Sciences, Romanian Academy, Timisoara Branch, 300223, Timisoara

Corresponding author: Sandor I. Bernad, E-mail: sbernad@mh.mec.upt.ro

We investigated the flow field within a rigid-walled numerical model of 30°, 45°, and 60° degree by-pass graft in order to attempt to identify different type of vortices developed in distal part of the by-pass graft. In steady laminar flow, the presence of branching generates a secondary flow in the form of a pair of counter-rotating symmetrical vortices called Dean cells. Velocity profiles and flow visualization images, were obtained numerically for all investigated by-pass angles. The secondary flow generated by centrifugal force, induce irregular fluid particle trajectories inside to the by-pass graft. For all investigated by-pass angles we have clearly demonstrated the complex nature of the flow pattern, and furthermore we have shown that there are significant differences between the flow fields and also the secondary vortex generated in each by-pass graft.

Key words: dean vortice, secondary flow, by-pass graft, numerical simulation.

NOMENCLATURE

D	[m]	graft inlet diameter	U	[m/s]	characteristic velocity
D_h	[m]	hydraulic diameter	U_m	[m/s]	mean axial velocity
De	[-]	nondimensional Dean number	V_{in}	[m/s]	inlet velocity
Re	[-]	nondimensional Reynolds number	ρ	[kg/m ³]	fluid density
H	[-]	helicity	τ_{ij}	[-]	viscous shear stress tensor
p	[Pa]	pressure	ν	[m ² /s]	kinematic viscosity
R_c	[m]	mean radius of curvature	μ	[Pa.s]	dynamic viscosity

1. INTRODUCTION

Curved channel flows and branching of fluid flow are used in many industrial applications to provide compactness and high heat and mass-transfer rates so as to enhance mixing in laminar flow regimes. Branchings of fluid flow are extremely common throughout the human body and involve various complex geometrical configurations and flow conditions associated with different ranges of Reynolds numbers, pulsatility and wall flexibility. Branchings greatly affect the fluid dynamics and are common sites of disease in human cardiac circulation.

The flow in curved and branching channels is characterized by a secondary flow in the form of a pair of counter-rotating symmetrical vortices in the pipe cross section, these corner vortices are called end cells or Eckman vortices by Finlay and Nandakumar [1] and they are a consequence of the pipe wall curvature. Their existence was shown analytically for the first time by Dean [2] in tubes of circular cross section. The commonly used control parameter for a flow in a curved duct is the Dean number, De , defined as:

$$De = \frac{U_m D_h}{\nu} \sqrt{\frac{D_h}{R_c}}, \quad (1)$$

where, U_m is the axial mean velocity, ν is the kinematic viscosity, D_h is the hydraulic diameter and R_c is the mean radius of curvature. The Dean number is therefore the product of the Reynolds number (based on axial mean velocity U_m through a pipe of hydraulic diameter D_h) and the square root of the curvature ratio. Note that the hydraulic diameter is defined a

$$D_h = \frac{4(\text{cross section area})}{\text{wetted perimeter}}. \quad (2)$$

Dean vortices are the result of centrifugal forces. They are present in a variety of practical applications including technological and physical problems: internal turbine blades, cooling passages, biological systems, ducting in internal combustion engines and heat exchangers. The first mathematical analysis made by Dean [2] shows the onset of a pair of counter-rotating vortex cells in a Newtonian fluid flow in a curved channel resulting from the interaction between centrifugal and viscous forces. The Dean number represents a ratio of the centrifugal forces to the viscous forces, and measures the intensity of the secondary flows.

The effects of vortices or vortical structures are particularly evident when considering both flow stability, and the processes of mixing and transport by the flow [3, 4, 5].

This paper presents a series of numerical simulations intended to determine whether the use of commercially available computational fluid dynamics (CFD) software may provide a viable alternative to the use of physical models for predicting the occurrence of vortices and vortical structures in branching pipe.

The objective of this paper is to examine the dynamics both of vortex motion and of particle transport in application of the branching vessels, namely in the by-pass graft, and to relate these to parameters such as geometry, unsteadiness and the mixing processes by the flow.

2. NUMERICAL APPROACH

Graft geometry. The authors have used simplified geometry (Fig. 1) for the by-pass graft model with graft angles of 30° , 45° , and 60° for the analysis of the flow and WSSs around the graft junction, and across the bed of the host tube. The internal diameter for the graft was taken to be $D = 25.4$ mm with a graft-tube diameter ratio of 1:1 (Figs. 1 and 2).

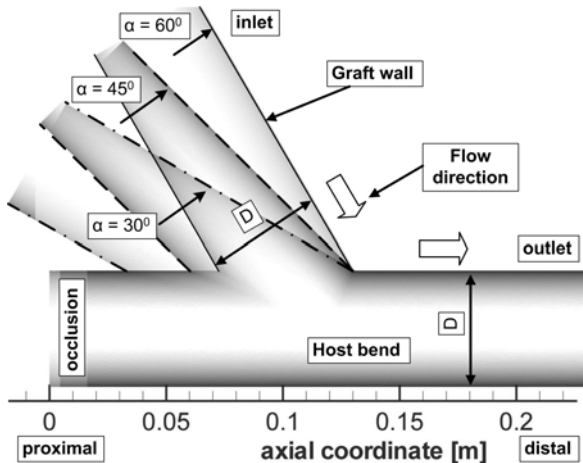


Fig. 1 – By-pass graft geometry along the longitudinal plane for three graft angles (30° , 45° and 60°).

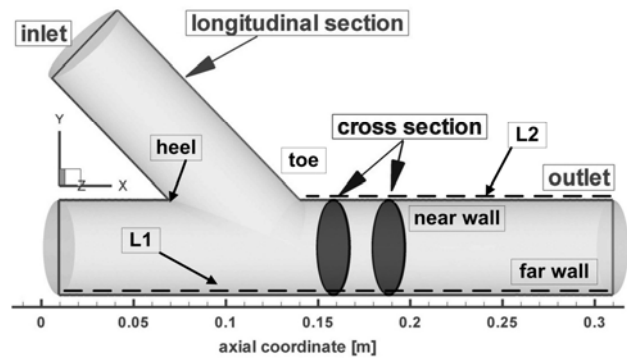


Fig. 2 – Different section used for hydrodynamic parameters investigation.

Assumptions. To simplify the analysis, fluid was assumed to be a homogeneous, incompressible and Newtonian. The simulations were carried out under steady flow condition, which is somewhat different from the pulsatile flow in vivo, but the results can still shed some light on the hydrodynamic performance of the grafts.

The steady, three-dimensional equations from the conservation of mass and momentum for an incompressible Newtonian fluid, form the basis of the numerical formulations for the flow analysis in a branching pipe.

The key assumptions for the numerical simulation of the flow are: steady state flow, flow is laminar, gravitational effects are negligible, and physical properties remain constant.

Governing equations. The flow can be described through the conservation laws, i.e. the conservation of mass, momentum and energy. As a reference the momentum equation in its general form (Eq. 3) is given in tensor notation and in Cartesian coordinates.

$$\underbrace{\frac{\partial}{\partial t}(\rho u_i)}_{\text{unsteady acceleration}} + \underbrace{u_j \frac{\partial}{\partial x_j}(\rho u_i)}_{\text{convective acceleration}} = \underbrace{\frac{\partial \tau_{ij}}{\partial x_j} - \frac{\partial p}{\partial x_i}}_{\text{divergence stress}} + \underbrace{\rho f_i}_{\text{other force}}, \quad (3)$$

Inertia

where p is the pressure, τ_{ij} the viscous shear stress tensor which is defined as:

$$\tau_{ij} = \mu \underbrace{\left(\frac{\partial u_i}{\partial x_j} + \frac{\partial u_j}{\partial x_i} \right)}_{\text{viscous shear stress}} - \mu \frac{2}{3} \delta_{ij} \frac{\partial u_k}{\partial x_k}. \quad (4)$$

The ratio of the inertia forces and the viscous forces acting on the fluid can be expressed in terms of non-dimensional Reynolds number:

$$\text{Re} = \frac{\text{inertial force}}{\text{viscous force}} = \frac{U \cdot D}{\nu}, \quad (5)$$

with ρ [kg/m³] denoting the fluid density, U [m/s] the characteristic velocity, D [m] diameter of the pipe, μ [Pa·s] the dynamic viscosity and ν [m²/s] the kinematic viscosity.

Boundary Conditions. Due to the elliptical nature of the flow conditions, boundary conditions must be specified at all the domain boundaries.

– *Inlet*: a uniform inflow velocity profile for the axial velocity component and a zero transverse velocity component are used. Here $V_{\text{inlet}} = 0.275$ m/s (based on Reynolds of 500).

– *Outlet*: the outlet pressure was defined to be 0 Pa.

– *Wall*: the vessel wall was assumed to be rigid and nonslip.

Incorporating above governing equations, a finite volume-based CFD model is formulated with the commercial package FLUENT [6] where SIMPLE algorithm is used for pressure-velocity coupling. The momentum and energy equations are discretised by first and second order schemes, respectively. Since the model considers both buoyancy and centrifugal source terms, pressure discretisation is performed with body force-weighted approach. The stability of the solution is monitored through continuity, velocity, pressure and dimensionless helicity where the convergence is achieved with values not higher than 10⁻⁶. Grid independency is carefully checked paying a special attention to the boundary layer modelling at the wall.

3. RESULTS AND DISCUSSION

Boundary layer separation is a well known phenomenon associated with sudden changes in surface geometry. The free shear layer resulting from a flow separation is likely to contain pressure, velocity and consequently local shear fluctuations which could be felt at the wall at the points of separation and of reattachment [7]. Also, the separation bubble itself, though, in general a vortex that is slower moving than the shear layer or the main flow, constitutes an area in which the wall could experience flow conditions different from those in other areas [8].

By-pass with 45° graft angle. In the occluded region of the 45 degrees by-pass model a vortical structure is evident when the recirculation is sufficiently strong to distinguish the particle motion from the rotational action of the boundary layers. (Fig. 3). When we increase the branch angle, however, the impact of the particles is sufficiently strong to generate a vortical structure not only in the occluded region but also at the sides of the junction leading to the looping structures.

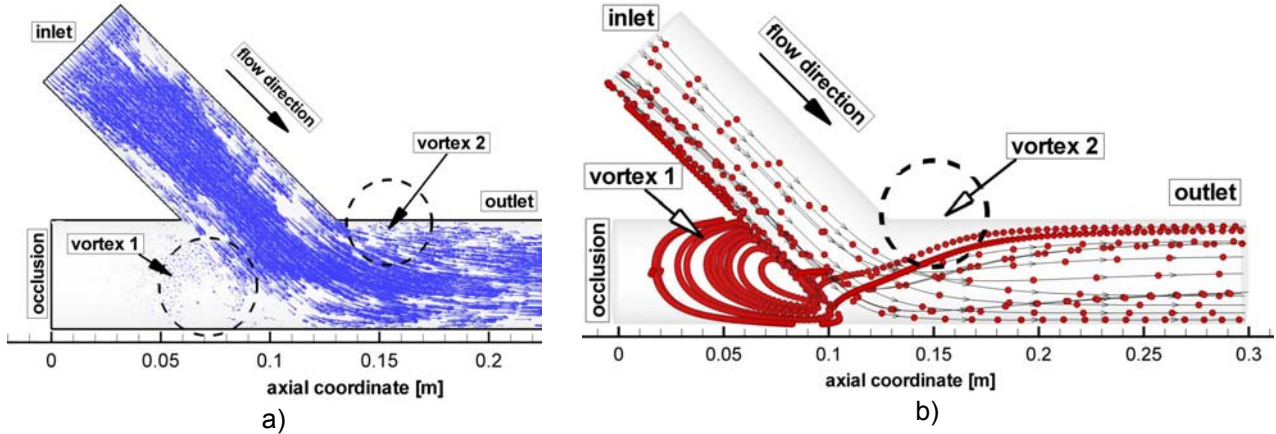


Fig. 3 – a) Velocity vectors along the longitudinale plane. Flowfields are shown for the 45° graft angle; b) three-dimensional view of the pathline of the high inertia fluid under steady flow conditions at $Re = 500$ showing development of the double helix.

Particle pathlines and streamlines coincide exactly for the case of steady laminar flow however, they may differ greatly in the case of transient flow. Most of this has to do with their respective nature; streamlines display a snapshot of the entire flow field at an instant in time, whereas particle pathlines trace the history of a particular fluid element through a region.

Just downstream of the toe, at $X = 0.15$ m, the axial velocity profile was skewed toward the far wall, and flow separation was observed along the near wall (Fig. 3). The trace at $X = 0.15$ m, clearly displayed the presence of secondary flow, which consisted of low inertia fluid swirling circumferentially around the vessel towards the near wall and the high inertia fluid from the core region being forced toward the far wall. Once the high inertia fluid approaches the far wall, it too travels circumferentially in a spiraling manner because of the centrifugal force generated by the change in flow direction (Fig. 3b).

Thus, at $X = 0.18$ m some of the high inertia fluid continued to move along the far wall while the remainder traveled around the vessel circumferentially in a double helical manner as shown in Figs. 3 and 5. For $Re = 500$, it appeared that the spiraling motion of the fluid (Fig. 5) created a high shear layer (a possible source of flow instability), that resulted in the formation of a small vortex just downstream of the toe of the anastomosis (Fig. 3). In other words, a small vortex was found to be embedded in the spiraling flow that consists of a main vortical motion superimposed on the axial flow.

Helicity. Figure 4 shows the area-weighted average helicity of the flow at twelve cross-sections of the each investigated by-pass grafts (between $X = 0.15$ m and $X = 0.3$ m), which can be used to compare the efficiency of the grafts in creating swirling flow. Helicity H and the area-weighted average of helicity H (*average*) were defined by the following equation:

$$H = (\nabla \times \vec{u}) \cdot \vec{u}, \quad (6)$$

As evident from Fig. 4, for all grafts, the helicity have a maximum degree at cross-section 1 (at $X = 0.15$ m), then starts to decrease gradually until cross-section 12 (at $X = 0.3$ m).

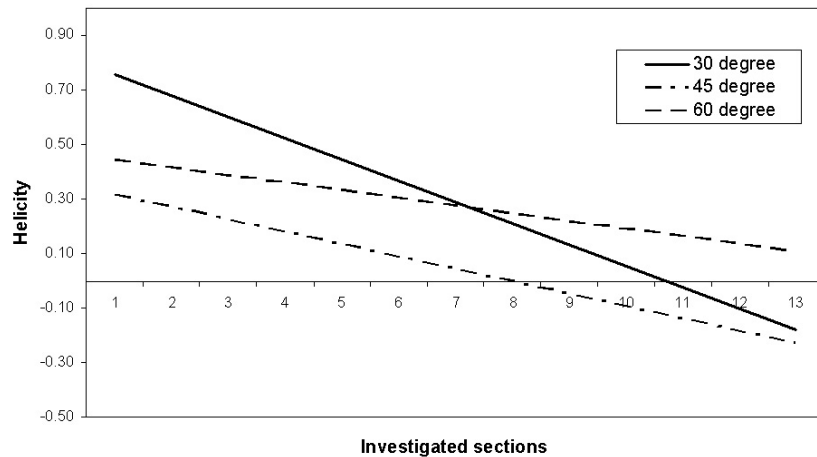


Fig. 4 – Helicity evolution at the twelve cross-sections (between $x = 0.15$ m and $x = 0.3$ m, Fig. 2) of the by-pass graft for all investigate junction angles. Helicity are normalized by the mean helicity in the outlet section.

The vorticity generation is proportional to the angular velocity vector of rotation, is influenced by circulation and stirring effects on fluid [9, 10]. In principle, mixing of fluids is a complex physical process that is governed by a convection-diffusion equation. However, in this study, mixing is simply regarded as stirring flow.

Fluid particles are mixed and make wide paths due to the combined effects of axial velocity and axial vorticity such as can be encountered when stirring coffee to melt sugar quickly.

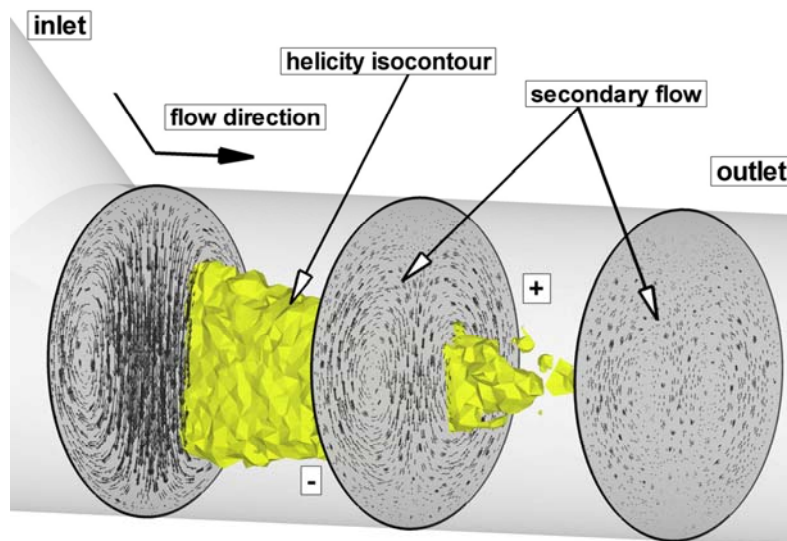


Fig. 5 – Secondary flow evolutions along the host bend distal to the toe in 45° by-pass geometry. Helicity iso-contour for helicity value of $He = 2$. Dean pair vortex: + clock wise direction, - anti-clock wise direction.

We carried out flow visualizations under the same conditions in the all investigated by-pass graft (with 30° , 45° and 60° by-pass angles) for Reynolds number ($Re = 500$). The results are shown in figure 6. The evolutions of the Dean cells are almost identical to those in the investigated cross-section at $X = 0.18$ m, but significant differ in each investigated graft angles.

For the Reynolds number studied here ($Re = 500$), we observed a secondary flow structure consisting of two counter-rotating cells along the whole geometry (Figs. 5 and 6).

The movement of the stagnation point can be appreciated from Figs. 5 and 7. For a branch angle of 45° degrees, as shown in Fig. 5, the stagnation point is biased toward the occluded region of the host and is located just proximal to the pipe intersections (Fig. 7).

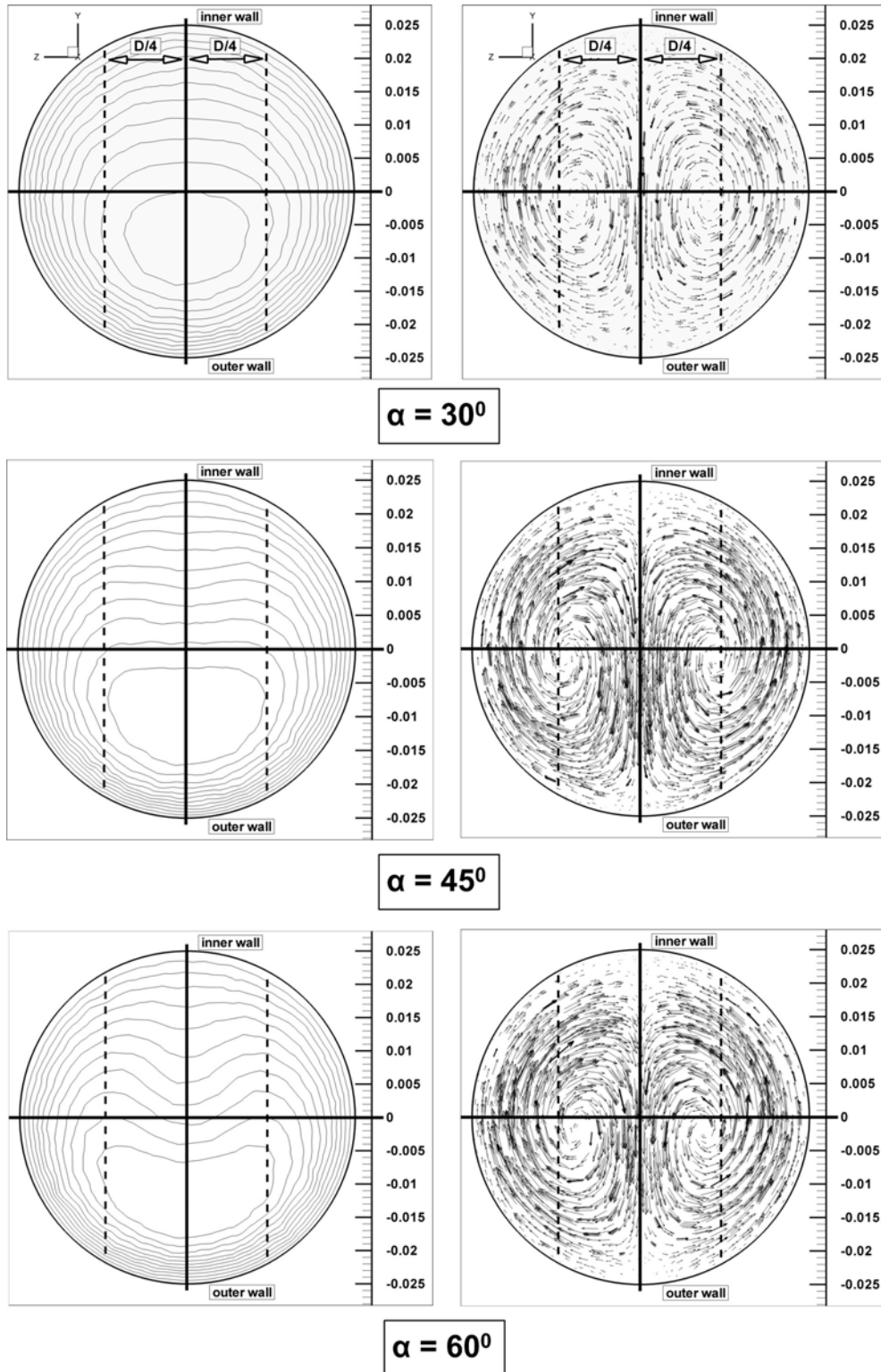


Fig. 6 – Flow visualization showing secondary flow for different by-pass angles for same cross-section $x = 0.18$ m (Fig. 2):
 a) axial velocity left; (b) secondary velocity vector right. Dean vortex center evolution for different by-pass angles.

The areas where low axial wall shear stress was observed included: (1) the near wall just beyond the toe of the junction, (2) the proximal region of the host vessel where an almost stagnant zone was seen, and (3) the stagnation point on the bed of the host vessel where the entry flow is split into the forward and retrograde flows (Fig. 7). Since the secondary flow caused by the centrifugal force is expected to be strongly

dependent on the angle of the graft, this geometric factor will influence the spatial and temporal variations of the velocity field.

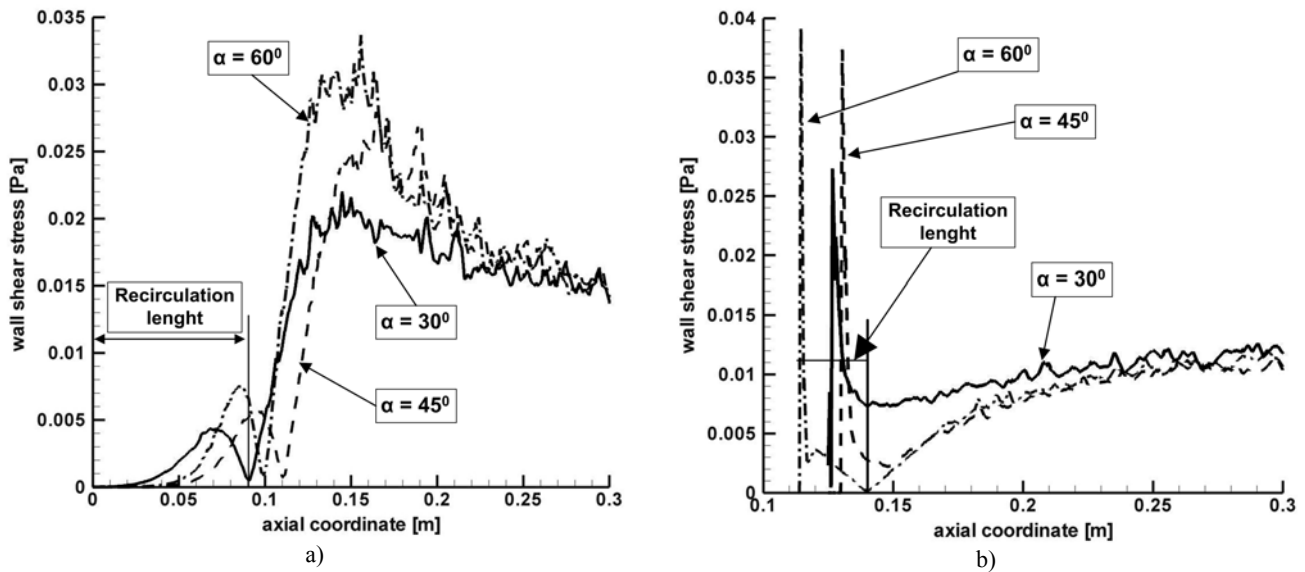


Fig. 7 – Wall shear stress – WSS and recirculation length evolution for different by-pass angles: a) WSS evolution along line L1 (far wall, Fig. 2); b) WSS evolution along line L2 (near wall, Fig. 2).

7. CONCLUSIONS

The most significant secondary flow features comprise the generation of Dean vortices in the distal host, a flow recirculation within an occluded host vessel and Dean vortex generation in the proximal host for bilateral host flows. The study has indicated that the dominant geometric effects on secondary flow arise through the branch angle and flow split both of which can cause flow separation opposite to the floor.

The increased angles also caused a flow separation at the toe region of the graft just proximal to the junction which is a potential site of the high particles residence time.

The present results can provide a better understanding of the effect of geometrical configurations of the by-pass graft on the hydrodynamic flow. Therefore, these results may provide practical applications by considering the mixing and wall shear stress distribution within by-pass graft model during the design and the modeling of a bypass graft vessel to enhance the mixing of the flow.

ACKNOWLEDGMENTS

This work has been supported by Romanian Academy annual program and work of Dr. Alin I. BOSIOC was supported by a grant of the Romanian National Authority for Scientific Research, CNCS – UEFISCDI, project number PN-II-RU-PD-2011-3-0165.

REFERENCES

1. FINLAY W.H., Nandakumar K., *Onset of two-dimensional cellular flow in finite curved channels of large aspect ratio*, Phys. Fluids A, **2**, 7, pp. 1163–1174, 1990.
2. DEAN W.R., *Note on the motion of fluid in a curved pipe*, Philos. Mag., **4**, pp. 208–223, 1927.
3. RAYZ V. T., BERGER S. A., SALOMER D., *Transitional flow in arterial fluid dynamics*, Comput. Methods Appl. Mech. Engrg., **196**, pp. 3043–3048, 2007.
4. OTTINO J.M., *Mixing, chaotic advection and turbulence*, Annu. Rev. Fluid Mech., **22**, pp. 207–253, 1990.
5. PELLEGRINI M., ENDO H., NINOKATA H., *Numerical investigation of bent pipe flows at transitional Reynolds number*, Progress in Nuclear Energy, **53**, pp. 916-920, 2011.

6. *** FLUENT 6.3 User's Guide, ANSYS-Fluent Incorporated, 2006.
7. JONES S.W., THOMAS O.M., AREF H., *Chaotic advection by laminar flow in a twisted pipe*, J. Fluid Mech., **209**, pp. 335–357, 1989.
8. CASTELAIN C., MOKRANI A., LEGENTILHOMME P., PEERHOSSAINI H., *Residence time distribution in twisted pipe flows: helically coiled system and chaotic system*, Exp. Fluids, **22**, pp. 359–368, 1997.
9. DOORLY D., SHERWIN S.J., *Geometry and flow*, in: Formaggia L., Quarteroni A., Veneziani A. (editors), *Cardiovascular Mathematics*, Vol. 1, Springer, 2009.
10. AREF H., *Stirring by chaotic advection*, J. Fluid Mech., **143**, pp. 1–21, 1984.

Received, May 20, 2013